Sensors and Materials, Vol. 12, No. 6 (2000) 365–373
MYU Tokyo

S & M 0415

Amorphous Silicon-Based Uncooled Microbolometer Technology for Low-Cost IRFPA

Astrid Bain, Jean-Luc Martin, Eric Mottin,
Jean-Louis Ouvrier Buffet, Jean-Luc Tissot,
Robert Tronel, Michel Vilain and Jean-Jacques Yon

DOPT/LIR - LETI/CEA. G 17, rue des Martyrs, 38054 Grenoble Cedex 9, France

(Received July 10, 2000; accepted September 18, 2000)

Key words: IRFpa, infrared focal plane array, amorphous silicon, uncooled microbolometer, thermal imaging

The Laboratoire InfraRouge (LIR) of the Laboratoire d'Electronique, de Technologie et d'Instrumentation (LETI) has been involved in the development of amorphous silicon uncooled microbolometer technology for several years. This paper reports progress that has been achieved in both technological and product fields. Due to the very particular features of LETI/ LIR technology, large fill factors, high thermal insulations, and small thermal time constants, can be achieved, resulting in a large detector responsivity. A model has been developed which accounts for these characteristics. Electro-optical results obtained from a laboratory prototype of 256 × 64 infrared detectors on a readout CMOS circuit (IRCMOS), with a 50 μm detector pitch, show a Noise Equivalent Temperature Difference (NETD) less than 50 mK at f/1 can be obtained even at a high video scanning rate (up to 100 Hz), compatible with microscanning techniques. This low-cost technology has been transferred to our industrial partner Sofradir and a new 320 × 240 array with a NETD value less than 80 mK is now available.

1. Background

The emergence of uncooled detectors has opened new opportunities for IR detection for both military and civil applications. Standard infrared applications are involved along with new applications that could not afford costly cooled detectors. Markets such as the automotive market require low production cost and high yield which can be achieved only using the silicon collective microelectronic process. LETI/LIR chose from the very

beginning to develop a monolithic bolometer technology fully compatible with commercially available CMOS technology. The resistive thermometer is based on amorphous silicon which is commonly used in microelectronics. We presented recently[1,2] a first demonstration of the qualities of our microbolometer devices. We have been working since then to simplify our process further and to master our technology for an easier and faster industrial transfer.

2. Technology

2.1 *Microbridge implementation*

Microbridges are built in a monolithic way over completed readout circuit substrates, thoroughly conventional microelectronics fabrication equipment (Fig. 1). In the first step a thin aluminum reflective layer is deposited and delineated directly on top of the readout integrated circuit (ROIC). A 2.5-μm-thick polyimide sacrificial layer is then spun and cured. A heavily doped amorphous layer silicon 0.1 μm thick is deposited over the polyimide layer and covered by 8 nm of titanium nitride by reactive plasma vapor deposition. Vias are opened by dry etching throughout the structure down to the ROIC pads, and metal deposition and etching achieves electrical continuity between the underlying substrate and the active bolometric structures at the surface of the polyimide. At this point electrode delineation is done by wet etching the titanium nitride layer selectively over the amorphous silicon. The pixel contour is then delineated and dry etched to the polyimide, and a final local polyimide etch over testing pads is carried out. At this stage the wafers are tested for standard automatic electrical functionality and acquisition of array parameters. Finally the microbridge arrays are released by polyimide removal in conventional resist ashing equipment.

2.2 *Detector engineering and design*

IR absorption is provided by controlling the titanium nitride layer resistance. The quarter-wavelength effect between the microbridge electrodes and the reflector roughly

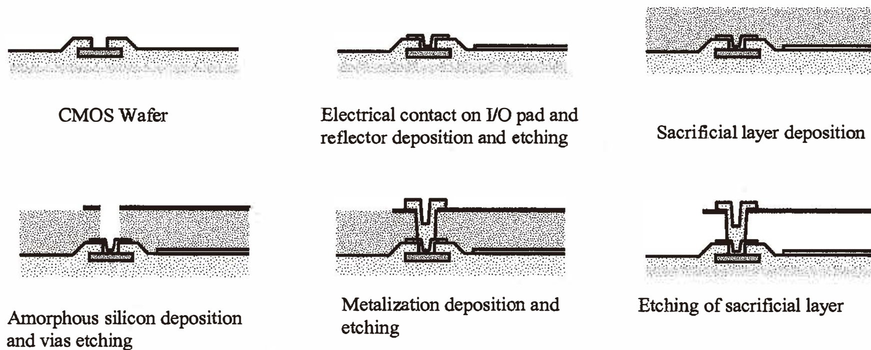

Fig. 1. Schematic of the process flow.

causes the response to peak in the 8–14 μm range. Amorphous silicon does not contribute much to optical absorption, except in parasitic interference effects. These effects tend to notch the spectral response due to the high refractive index of silicon. Thin layers (0.1 μm or less) are therefore preferred. These arrangements, combined with general 1.5 μm design rules, lead to spectral band absorption by a fill factor product of about 60%.

Thermal resistance is achieved by four thin legs per pixel, anchored to the substrate by metal studs formed by the metallized vias. At first, we developed structures with only two legs to sustain the amorphous silicon membrane. These structures provided adequate thermal resistance but were not mechanically reliable: microbridges tended to stick to the substrate when electrically activated. This problem was solved by the four leg design, as represented in the SEM view in Fig. 2. Thermal resistance loss due to doubling the number of anchoring points has been compensated, or even improved, by design rule shrinkage. Four 1.25-μm-wide, 0.1-μm-thick (neglecting titanium nitride), 12-μm-long legs lead to a global 1.5×10^7 K/W thermal insulation given the low thermal conductance of amorphous silicon. The highest levels of doping of the amorphous silicon thermometer have demonstrated the best results in terms of signal-to-noise ratio. Furthermore, these materials are easier to control in terms of deposition kinetics, uniformity and resistivity than less doped ones. Typical 120 Ω·cm and 2.4%/K TCR (at room temperature) amorphous silicon is routinely obtained with standard deposition equipment and in-house developed processes. Figure 3 shows the stability of the amorphous silicon resistivity in the different runs we processed.

These results prove the reliability of our deposition control for the thermometer. A good uniformity (std.dev./mean) of less than 7% is routinely achieved on each technological run associated with a spatial uniformity (std.dev./mean) better than 3% across each 4" wafer. Figure 4 shows the TCR behavior of the amorphous silicon layer from batch to batch. Material with a low excess of low-frequency noise and without random telegraph switching (RTS) noise is obtained by controlling the deposition. The contacts between the electrodes and the amorphous silicon are ohmic, thus reducing fluctuation in the dynamic resistance of the detector and also avoiding excess contact noise.

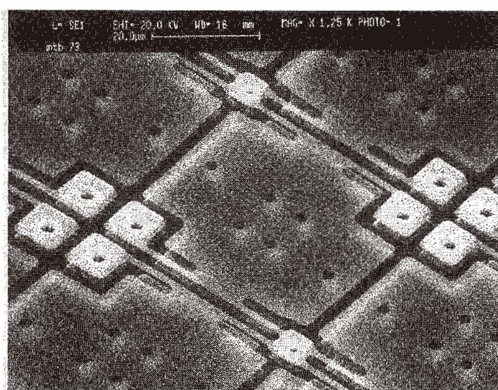

Fig. 2. SEM view of a pixel with four legs.

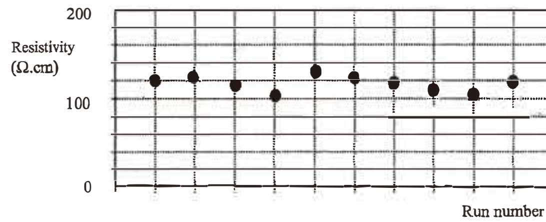

Fig. 3. Average resistivity of amorphous silicon across a 4" wafer.

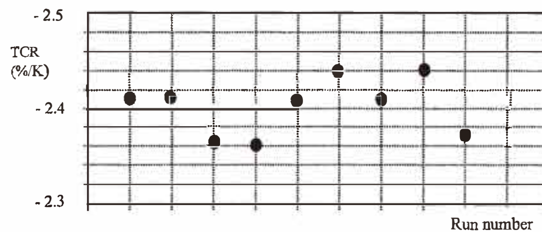

Fig. 4. Process control chart for the average TCR of amorphous silicon across a 4" wafer.

3. Readout Circuit and Modeling

In 1997 we developed a readout circuit which is still used as a test vehicle for our microbolometer technology. This readout circuit is a 256 × 64 focal plane array. The pixel implementation is presented in Fig. 5. Each detector Rd is coupled with a direct current injection into transistor Md. Both continuous and pulsed supply modes are possible. In continuous mode, the SR switch is "on" during integration. When the row is not addressed by the row multiplexer, the bolometers are still biased by SB switches in the "on" state. In pulsed mode, the bolometer is powered by SR uniquely during the integration time; the SB switch is never "on." Most of the background current is suppressed using one or more blind bolometers Rb for each column. The useful current from the bolometer is then integrated into a capacitive transimpedance amplifier (CTIA) at the bottom of the column.

The 2D arrangement of the matrix needs a multiplexer circuit to select individual pixels. The 256 × 64 focal plane array (FPA) circuit configuration is shown in Fig. 6. The FPA is read on a row by row basis.

Along with the readout circuit, we have developed a model to determine precisely the performance of its components under any conditions. This model helps orientation of the technological development, tuning the current circuit to get optimum performance and also helps in the design of new optimized architectures and application-specific readout circuits. This model has been fully validated on a previous test chip. We will now describe the basis of this model.

The physical phenomena taken into account in the model are the following:

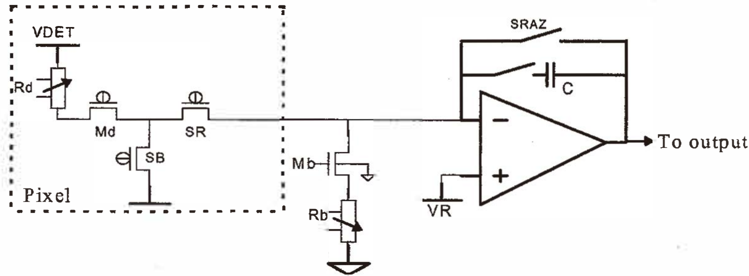

Fig. 5. Pixel configuration.

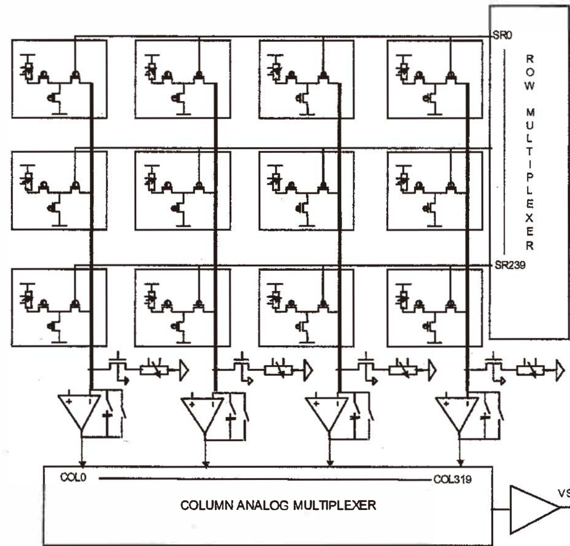

Fig. 6. Implementation of readout IC array.

- the properties of IR flux,
- the absorption of the electromagnetic wave by the detector,
- the intrinsic electrical characteristics of bolometric resistance,
- the coupling between electrical and thermal phenomena.

The equations we present below cover the circuits based on bolometer voltage polarization. The bolometer acts as a thermal RC filter as shown in Fig. 7. It is controlled by the following differential equation:

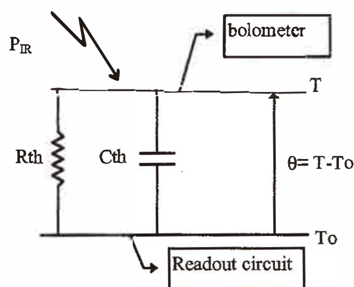

Fig. 7. Bolometer model.

$$\frac{\theta}{R_{th}} + C_{th}\frac{d\theta}{dt} = P_{joule} + P_{ir},$$

where θ is the temperature difference $T-T_o$ between the bolometer microbridge and the readout circuit and R_{th} and C_{th} are the thermal resistance and thermal capacitor, respectively. P_{joule} is the electrical power dissipation and P_{ir} the absorbed infrared power.

The signal-to-noise ratio is the criterion to maximize to achieve the best detector performance. To calculate this ratio, we integrate the noise current spectral density in the readout circuit bandwidth (which depends on the integration time). Our model, detailed elsewhere,[3] leads to the following curves (Fig. 8) which show the evolution of the signal-to-noise ratio with electrical power dissipation in the bolometer in both pulsed and continuous mode. In ref. (3), we demonstrated the dependence of the responsivity and the 1/f noise on bias voltage. From these equations, the signal-to-noise ratio (s/n) can be evaluated with bias voltage level, and a saturation of s/n appears with high values of bias power dissipation.

As can be seen, both modes lead roughly to the same performance limited by 1/f noise. To achieve this performance, polarization must be higher in the pulsed mode.

The pulsed mode, however, has many significant advantages. Consumption in the detector is reduced as the detectors are only polarized during the integration phase. This is obviously a key point in the design of portable systems for which battery weight and autonomy are critical. The pulsed polarization also reduces the component vulnerability and preserves the intrinsic time constant of the detector (4 ms). This time constant is suitable with 30, 60 and even 120 Hz frame rate imagery. The remanence associated is respectively –80 dB, –40 dB and –20 dB, enabling, for example, the use of microscanning techniques. Finally, the pulsed mode presents a reduced sensibility to focal plane temperature fluctuations because the blind bolometer allows a better compensation for focal plane temperature fluctuation since its temperature is almost the same as the active pixel one.

For these reasons, LETI/LIR is now currently working on a pulsed bias mode circuit. The performance achieved is summarized in the following paragraph.

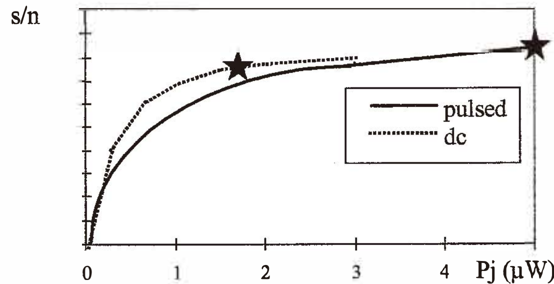

Fig. 8. Evolution of the signal-to-noise ratio with electrical power dissipation.

4. Results

4.1 *Electro-optical performance*

A 256 × 64 bolometer uncooled IRFPA chip was integrated into a vacuum package and placed at the focal plane of an IR camera. The signal from the IRFPA was corrected for nonuniformity in bolometer resistance and responsivity by viewing an extended area blackbody source at two temperatures. The histogram of the focal plane responsivity for 300 K blackbody irradiance is shown in Fig. 9(a). The mean value is approximately 10 mV/K and the response uniformity is less than 10% (σ/μ). As shown in Fig. 9(b), a NETD of 50 mK (for f/1 aperture and 25 Hz imagery frequency) has been demonstrated at an FPA operating temperature of 295 K. This NETD is only slightly affected (60 mK instead of 50 mK) by 100 Hz image frequency. This loss in performance is mainly due to the readout circuit which was not optimized for such a rate.

4.2 *Automotive demonstration*

This laboratory device has been tested as enhanced driver vision for an automotive application. Two recorded scenes taken from the video tape are shown in Fig. 10. These images were taken from a standard camcorder and from our IR microbolometer camera securely fixed on the roof rack of a car. The left images are obtained at day time and show no additional useful information for the driver. On the other hand, the right images show a jogger running at night with his dog along a small country road with a car coming with high beam head lamps on. The blooming of the visible CCD image is to be compared with the quality of IR microbolometer image which shows very useful additional information to the driver.

About 50 components were integrated and tested in the last few months and the operability is now routinely better than 99.9%. Operability is defined as the percentage of pixels whose NETD is less than twice the chip mean NETD value. These results show the maturity of our standard technology, which has been transferred this year to our industrial partner Sofradir.

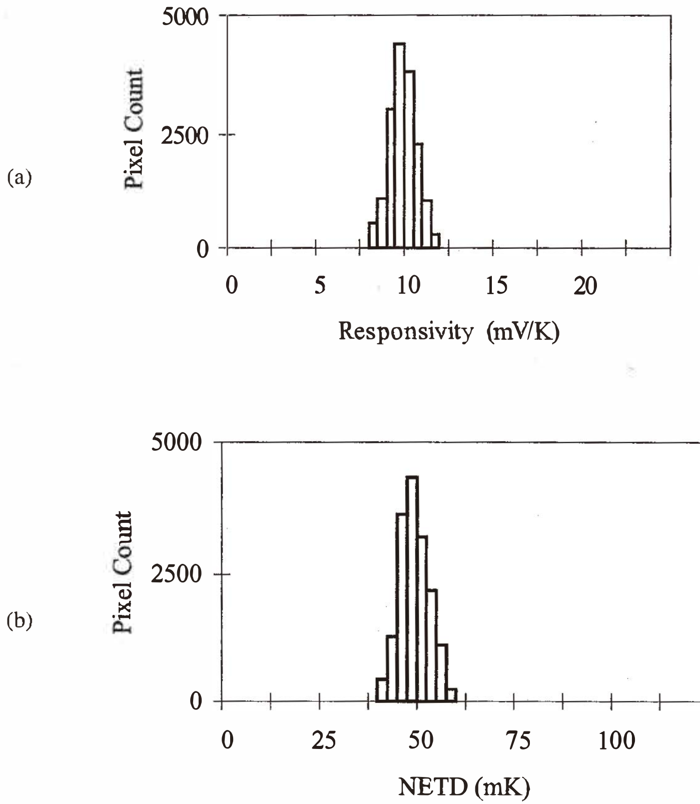

Fig. 9. (a) Responsivity histogram of a 256 × 64 device and (b) NETD histogram.

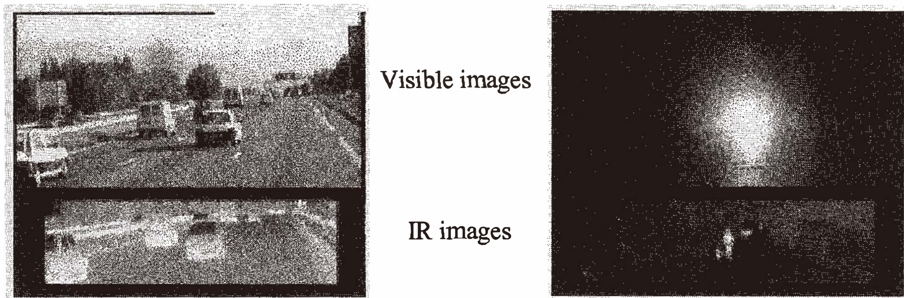

Fig. 10. 256 × 64 IR image and visible CCD image comparison.

5. Conclusions

We have presented in this paper the state of the art of our technology in terms of manufacturing and performance. We have also explained the main features of our model, which is a key tool for optimizing future technological choices and circuit designs. Equations for the signal-to-noise ratio allow us to determine the best operating conditions for the readout circuit (bias voltage integration time) and sustain the technological development orientation (thermal resistance, 1/f noise coefficient). The next-generation readout circuit has already been implemented and wafer fabrication is now providing 2D arrays. This new IRFPA is a 320×240 array with a pixel pitch of 45 μm. The performance is better than 80 mK for an image frequency of 30 Hz.[4] This product is being commercialized by our industrial partner Sofradir.

Acknowledgments

The authors thank the DGA/DTCO and the CEA for supporting these studies and the staff of the LETI/LIR who took part in them.

References

1 J. L. Tissot, F. Rothan, C. Vedel, M. Vilain and J. J. Yon: SPIE **3379**, Infrared Detectors and Focal Plane Arrays V (Orlando, USA, 1998).
2 J. L. Tissot, F. Rothan, C. Vedel, M. Vilain and J. J. Yon: SPIE **3436**, Infrared Technology and Applications XXIV (San Diego, USA, 1998).
3 C. Vedel, J. L. Martin, J. L. Ouvrier-Buffet, J. L. Tissot, M. Vilain and J. J. Yon: IRFPA SPIE **3698** Infrared Technology and Application XXV (Orlando, Cal, USA, 1999).
4 J. L. Tissot, J. L. Martin, E. Mottin, M. Vilain, J. J. Yon and J. P. Chatard: 320 × 240 Microbolometer Uncooled IRFPA Development, to be published in SPIE **4130** (San Diego, USA, 2000).